Short Communication

In-situ Monitoring of Internal Temperature, Flow Rate and Pressure in the High-temperature Proton Exchange Membrane Fuel Cell Stack using Flexible Integrated Micro Sensor

Chia-Hung Chen[1], Chi-Yuan Lee[2,*], Fang-Bor Weng[2], Shyong Lee[1], Yen-Ting Huang[2], Yen-Ting Cheng[2] and Chih-Kai Cheng[2]

[1]Department of Mechanical Engineering, National Central University, Taoyuan, Taiwan, R.O.C.
[2]Department of Mechanical Engineering, Yuan Ze Fuel Cell Center, Yuan Ze University, Taoyuan, Taiwan, R.O.C.
[*]E-mail: cylee@saturn.yzu.edu.tw

During the chemical reaction process of high-temperature proton exchange membrane fuel cell (HT-PEMFC) stack, the non-uniformity of internal local temperature, flow rate and pressure would result in poor membrane durability, fuel distribution non-uniformity and adverse impact on the fuel cell stack performance and service life. This paper applies the micro-electro-mechanical systems (MEMS) technology to develop flexible integrated (temperature, flow rate and pressure) micro sensor resistant to the high-temperature electrochemical environment. Appropriate materials and processing parameters are selected to protect the integrated micro sensor from failure or damage in long term test. The internal local temperature, flow rate and pressure are monitored in real time. The proposed design has advantages of three sensing functions, compactness, acid corrosion resistance, good temperature tolerance, short response time, *in-situ* measurement and applicability to any position.

1. INTRODUCTION

The high-temperature proton exchange membrane fuel cell stack (HT-PEMFC stack) is characterized by portable application, high energy conversion efficiency, no electrolyte loss, easy assembly and production and long operation life [1]. In the past decade, research teams around the world have paid particular attention to HT-PEMFC stack (120~200°C) [2-4].

At present, the development of fuel cell technology is mainly low temperature proton exchange membrane fuel cell stack (LT-PEMFC stack). The bottlenecks of low temperature fuel cell stack

include (1) the anode catalyst has poor CO poisoning resistance in low temperature (<80°C) environment; (2) the perfluorosulfonic acid membrane has good ionic conductivity only in high humidity environment; (3) high cathodic reduction overpotential; (4) liquid water and heat removal management [5], so that the bulk production schedule is delayed. Therefore, the latest international trend, such as U.S. DOE (Department of Energy), EU and Japan NEDO (New Energy Development Organization) develop towards high temperature fuel cell technology. However, the problems in the high temperature fuel cell stack, such as membrane material durability, catalyst corrosion, local flow, pressure and temperature nonuniformity inside the fuel cell stack, should be addressed to commercialize the fuel cell stack. The internal information of fuel cell stake can be discussed by using external measurement, invasive, theoretical modeling and single temperature, flow and pressure measurement. However, the aforesaid methods have some problems, such as too large volume of detector, measurement inaccuracy, influencing the fuel cell stack performance and unknown internal actual reactive state. Luke [6] used a self-made measuring plate to invade a high temperature fuel cell stack to measure the temperature, and compared it with simulation. Zhao [7] proposed the thermal management model and simulated the temperature, voltage and flow rate in the fuel cell. Kang [8] designed the numerical model of the rate in high temperature proton exchange membrane fuel cell, and simulated the temperature distribution in the fuel cell. This paper applies the micro-electro-mechanical systems (MEMS) technology to develop flexible integrated (temperature, flow rate and pressure) micro sensor resistant to the high-temperature electrochemical environment. The real-time microscopic monitoring of local temperature, flow and pressure in the high temperature proton exchange membrane fuel cell stack is the topic of this study.

2. SENSING PRINCIPLE OF FLEXIBLE INTEGRATED MICRO SENSOR AND EXPERIMENTS

2.1 Sensing principles of micro temperature sensor
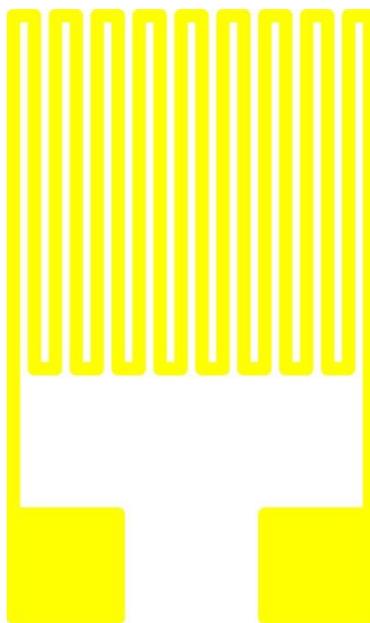
Figure 1. Schematic diagram of design of micro temperature sensor.

The design of micro temperature sensor is shown in figure 1. The sensing principle is that when the ambient temperature rises, as gold has positive temperature coefficient (PTC), the resistivity increases, this characteristic is resulted from the "temperature coefficient of resistance" (TCR) of conductor, defined as Eq. (1).

$$\alpha = \frac{1}{\rho_0}\frac{d\rho}{dT} \tag{1}$$

Eq. (1) shows the relationship between the temperature and resistance value of conductor is nonlinear, but if the resistance temperature detector is used in the linear range of resistance value of conductor, Eq. (1) can be reduced to Eq. (2).

$$R_t = R_r(1 + \alpha_1 \Delta T) \tag{2}$$

where the physical significance of temperature coefficient α_1 is the sensitivity of micro sensor, so Eq. (2) can be changed to Eq. (3).

$$\alpha_1 = \frac{R_t - R_r}{R_r(\Delta T)} \tag{3}$$

2.2 Sensing principle of micro flow sensor

The hot-wire micro flow sensor is designed according to the positive correlation between the thermal energy dissipation rate of hot wire and fluid flow. The sensing principle of hot-wire micro flow sensor is shown in figure 2.

According to King's law, the relationship between thermal energy dissipation rate and fluid flow rate is expressed as Eq. (4).

$$Q = I^2 \times R = I \times V = (A + B \times U^n)(T_s - T_o) \tag{4}$$

where Q is the electric power supplied from external power supply; U is the flow rate of fluid; n is the coefficient of correlation between heat Q and flow rate U, it is about *0.5* according to experiment; T_s is the temperature of hot wire; T_o is the temperature of inlet fluid; A is constant, the coefficient of heat transmitted by heater when the flow is fixed at zero; B is constant, the coefficient of heat from fluid and heater when the flow is not zero. Therefore, Eq. (4) can be changed to Eq. (5).

$$Q = (A + B \times U^{0.5})\,\Delta T \tag{5}$$
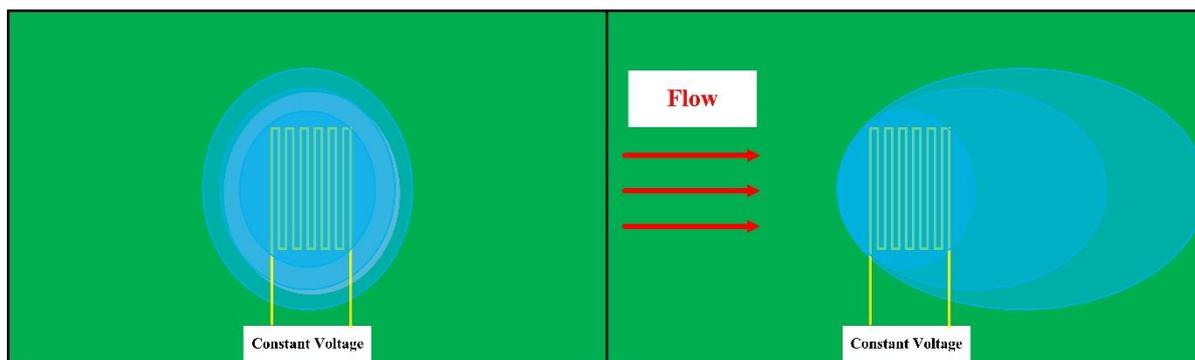
Figure 2. Schematic diagram of sensing principle of micro flow sensor.

2.3 Sensing principle of micro pressure sensor

The structure of capacitive micro pressure sensor is a nonconducting dielectric layer sandwiched in between two parallel electrodes. The capacitance value is calculated as Eq. (6).

$$\Delta C = \varepsilon_r \varepsilon_0 \frac{A}{\Delta d} \qquad (6)$$

where ε_r is the dielectric constant of material, ε_0 is the constant 8.854×10^{-12} (F/m), A is the projection overlapping area of two parallel electrodes, Δd is the vertical distance variation between two parallel electrodes. According to Eq.(6), the dielectric constant and the projected area of two parallel electrodes only influence the initial capacitance value, the capacitance variation is influenced mainly by the variation of distance between two parallel electrodes.

If one electrode structure is deformable membrane, the dielectric layer is sensor of air or vacuum hollow structure, the capacitance is calculated as Eq. (7).

$$\Delta C = \int\int \frac{\varepsilon}{d - w(x, y)} dx dy - C_0 \qquad (7)$$

where w(x,y) is the function of x-y deformation of membrane.

In order to enable the capacitive micro pressure sensor to present linear response, the sensitivity is increased and the process convenience is considered. The dielectric layer material of micro pressure sensor in this study is Fujifilm Durimide® PI 7320 with suitable stiffness, dielectric constant, elastic coefficient and process convenience. As the cavity between two parallel plate electrodes is replaced by polymers, the deformation of membrane electrode is average. In addition, the dielectric constant of PI 7320 is 3.2, in comparison to air dielectric constant 1. The micro pressure sensor has larger initial capacitance, and the capacitance variation is increased. Thus, the sensitivity is enhanced, facilitating micro pressure sensor correction and measurement [9]. In order to locate the micro pressure sensor in the runner of high temperature fuel cell stack, the runner size is 1.1mm×1.1mm. If the micro pressure sensor is too large, the micro pressure sensor is likely to be pressed and destroyed or the measurement of micro pressure sensor is obstructed. Therefore, the capacitive sensing area is designed as 800μm×800μm, as shown in figure 3.
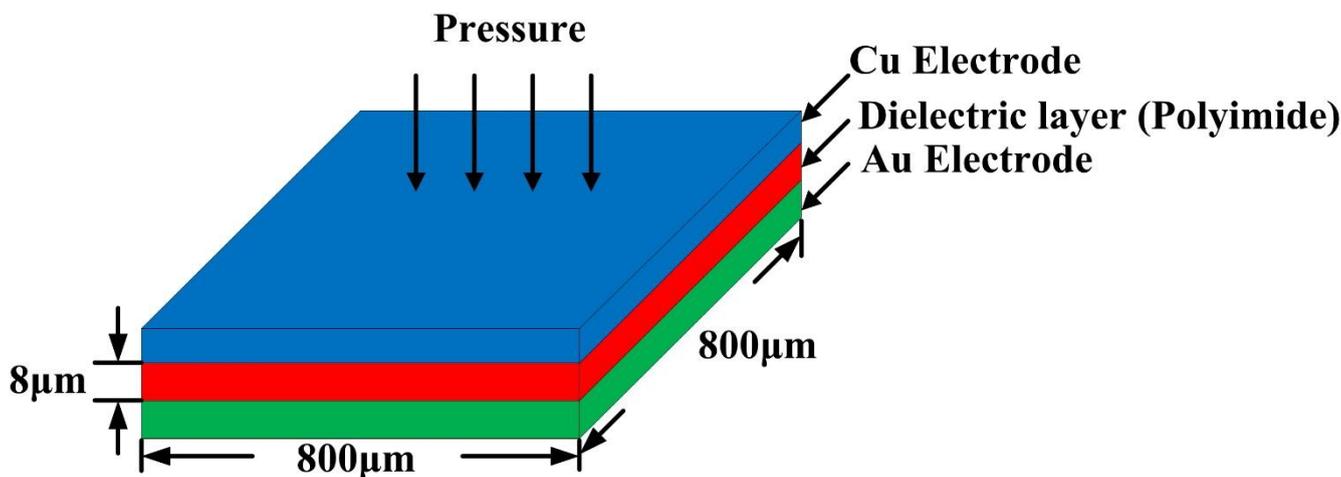
Figure 3. Schematic diagram of design of capacitive micro pressure sensor.

2.4 Experiment conditions

The testing of high temperature fuel cell stack is testing by 500 W PEM Fuel Testing Station 890C testing machine. When the fuel cell stack temperature is 160°C, the anode and cathode plates are given different unhumidified gas flows. In the case of constant current (5, 13, 20A) for different loads, the actual data and variation of local temperature in the fuel cell stack are obtained by instant and continuous measurement of NI PXI 2575 data acquisition system, the detailed operating conditions are shown in table 1. This experiment is carried out when the temperature and open circuit voltage (OCV) of fuel cell stack are stable.

Table 1. Test conditions for HT-PEMFC stack.

Subject	Specification
Stack temperature (°C)	160
Flow rate (H_2) of anode (slpm)	5
Flow rate (Air) of cathode (slpm)	30
Gas temperature	Room temperature
Constant current (A)	5, 13, 20

3. RESULTS AND DISCUSSION

3.1 Local temperature distributions in different cells

Figure 4 shows the local temperature in different cells. It is observed that the temperature increases gradually with the constant current (5, 13, 20A), as the higher the operating current is, the higher is the heat released from chemical reaction, and in the case of high current (20A), the thermal distribution nonuniformity becomes worse gradually. The temperature of Cell 10 is apparently lower than that of other cells, because the 3-in-1 micro sensor is close to the metal collector plate. The heat dissipation is fast, and the cathode terminal gas flow is high, it is room temperature when the gas is led in, so that the temperature of Cell 10 is lower. The temperature of Cell 5 is higher, it may because Cell 5 is located in the center of high temperature cell stack. The gases on both ends take the heat from the front end to the tail end. The internal chemical reaction is drastic in the case of high current (20A), and there is heat concentration, so that the temperature of Cell 5 is higher than other cells. Siegel [10] placed 36 resistance temperature detectors (RTD) on the cathode current collector plate of the high temperature fuel cell for external measurement, the experimental results showed the thermal distribution is nonuniformity. Lee [11] under the condition of constant current at 12A and output for 30 min, real-time monitoring was conducted on the temperature. The experimental results showed the temperature is stable.
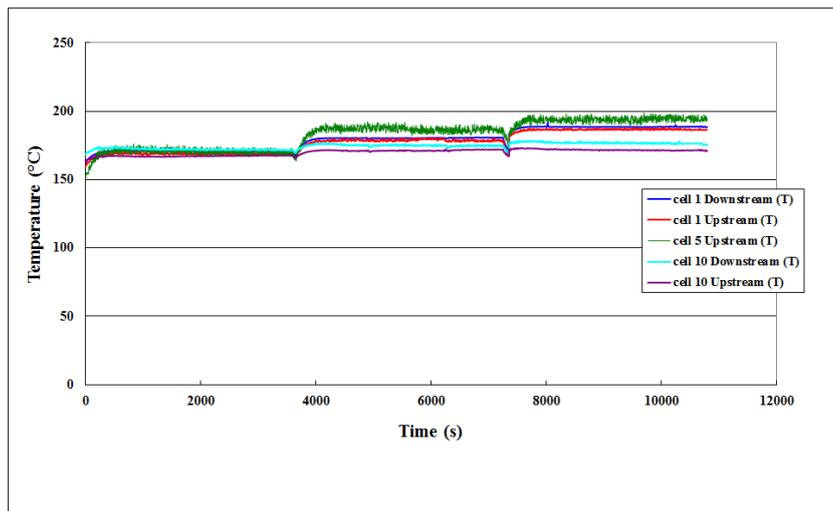
Figure 4. Comparison diagram of local temperature and voltage in different cells.

3.2 Local flow rate distribution in different cells

Figure 5 shows the local flow in different cells. It is observed that the upstream flow is higher than the downstream, and Cell 1 and Cell 10 are higher than Cell 5. Because the upstream flow of Cell 1 and Cell 10 is nearby the air inlet, the gas is sufficient. The downstream flow is lower, because the high temperature cell stack uses multiple snakelike runners in order to have better performance, the internal gas distribution is nonuniform, so that the downstream flow is lower. The flow of Cell 5 is lower than Cell 1 and Cell 10. This is because the Cell 5 is located in the center of high temperature cell stack, and the gases on both ends are taken through single cells from the front end to the center. The flow is lost partially through each cell, so that the flow of Cell 5 is lower than other cells.
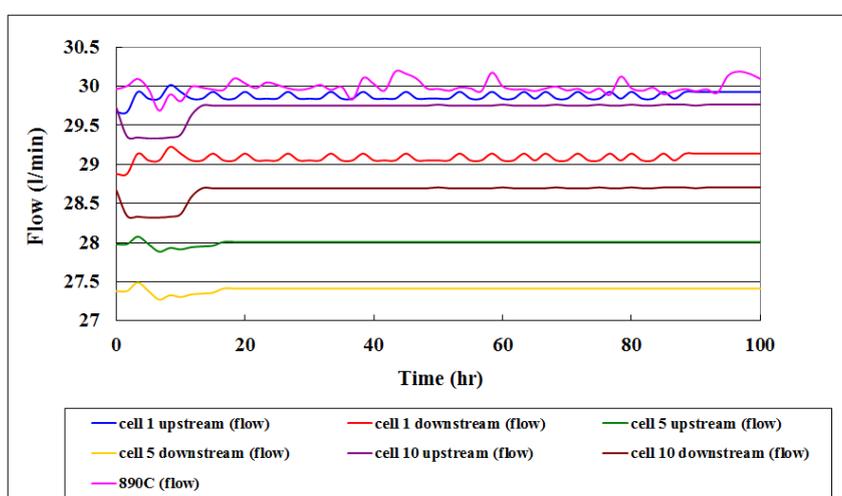
Figure 5. Comparison diagram of local flow in different cells.

3.3 Local pressure distribution in different cells

Figure 6 shows the local pressure in different cells. It is observed that the local pressure in the high temperature cell stack does not vary as the constant current (5, 13, 20A) increases.
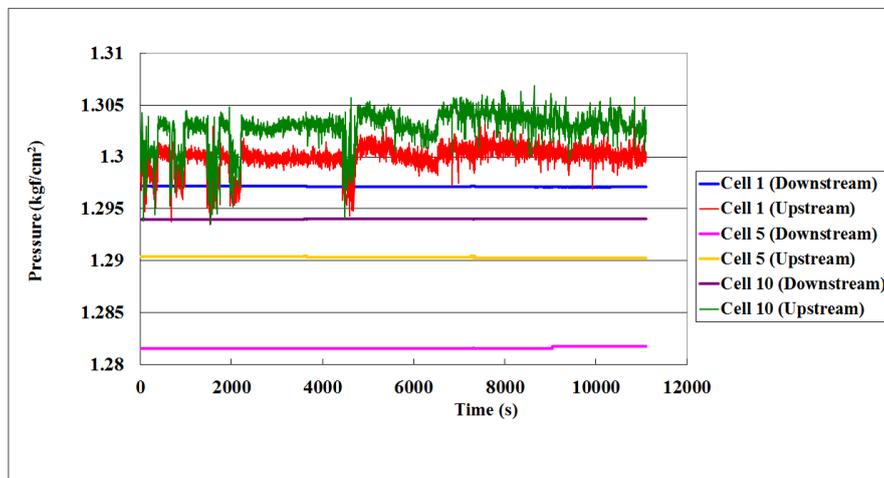
Figure 6. Comparison diagram of local pressure in different cells.

The downstream pressure is slightly higher than the upstream pressure. The average pressure in the high temperature cell stack is 1.25atm. The upstream pressure value of Cell 1 and Cell 10 fluctuates up and down. This is because the flexible integrated micro sensor is close to the air inlets on both ends of cell stack, and the cathode terminal gas flow is high. Moreover, the upstream end pressure of Cell 1 and Cell 10 is unstable. It is stabilized at the downstream end. The upstream-downstream end pressure difference of Cell 5 is small, meaning the pressure in the high temperature cell stack is stable. It can be used to evaluate whether the design of internal flow field of high temperature cell stack is good or not.

4. CONCLUSIONS

This study used MEMS technology to develop a high temperature electrochemical environment resistant integrated (temperature, flow and pressure) micro sensor on 40μm thick stainless steel substrate. The protection layer is made of PI with better temperature tolerance. This high temperature electrochemical environment resistant integrated micro sensor has three functions. It is characterized by compactness, acid corrosion resistance, good temperature tolerance, quick response, real-time measurement and arbitrary location.

The local temperature, flow and pressure information inside the high temperature fuel cell stack are extracted successfully. The test result of operating temperature 160°C and constant current (5, 13, 20A) shows that the nonuniform temperature and flow distributions in the high temperature fuel cell stack.

References

1. H. Janssen, J. S. Lueke, L. W. Lenhnert, D. Stolten, *Int. J. Hydrogen Energy,* 38 (2013) 4705-4713.
2. J. Zhang, Z. Xie, J. Zhang, Y. Tang, C. Song, T. Navessin, Z. Shi, D. Song, H. Wang, D. P. Wilkinson, Z. S. Liu, S. Holdcroft, *J. Power Sources,* 160 (2006) 872-891.
3. Q. Li, J. Q. Jensen, R. F. Savinell, N. J. Bjerruma, *Progess in Polymer Science,* 34 (2009) 449-477.
4. A. Chandan, M. Hattenberger, A. E. Kharouf, S. F. Du, A. Dhir, V. Self, B. G. Pollet, A. Ingram, W. Bujalski, *J. Power Sources,* 231 (2013) 264-278.
5. S. Bose, T. Kuila, T. X. H. Nguyen, N. H. Kim, K. T. Lau, J. H. Lee, *Progess in Polymer Science,* 36 (2011) 813-843.
6. L. Luke, H. Janßen, M. Kvesi, W. Lehnert, D. Stolten, *Int. J. Hydrogen Energy,* 37 (2012) 9171-9181.
7. X. Zhao, Y. Li, Z. Liu, Q. Li, W. Chen, *Int. J. Hydrogen Energy, 40* (2015) 3048-3056.
8. T. Kang, M. Kim, J. Kim, Y. J. Sohn, *Int. J. Hydrogen Energy,* 40 (2015) 5444-5455.
9. C. C. Chiang, C. K. Lin, M. S. Ju, *Sensors and Actuators A,* 134 (2007) 382-388.
10. C. Siegel, G. Bandlamudi, A. Heinzel; *Int. J. Hydrogen Energy,* 36 (2011) 12977-12990.
11. C. Y. Lee, S. J. Lee, Y. M. Lo, Y. M. Liu, *Int. J. Electrochem.. Sci.,* 9 (2014) 272-281.